Damage Localization on Composite Structures Based on the Delay-and-Sum Algorithm Using Simulation and Experimental Methods

Cedric Bertolt Nzouatchoua, Mourad Bentahar, Silvio Montresor, Nicolas Colin, Vincent Le Cam, Camille Trottier, Nicolas Terrien

MDPI

Article

Damage localization on composite structures using new methods based on the delay-and-sum algorithm

Cedric Bertolt Nzouatchoua [1,2,3], Mourad Bentahar [1], Silvio Montresor [1], Nicolas Colin [2], Vincent Le Cam [3], Camille Trottier [2] and Nicolas Terrien [2]

[1] Laboratoire d'Acoustique de l'Université du Mans (LAUM), UMR CNRS 6613, Institut d'Acoustique—Graduate School (IA—GS), CNRS, Le Mans Université, 72085 Le Mans, France; e-mail@e-mail.com
[2] IRT Jules Verne – NANTES UNIVERSITE – Institut de Recherche Technologique Jules Verne; e-mail@e-mail.com
[3] Université Gustave Eiffel, COSYS-SII, I4S, Bouguenais, France; e-mail@e-mail.com
* Correspondence: e-mail@e-mail.com; Tel.: (optional; include country code; if there are multiple corresponding authors, add author initials) +xx-xxxx-xxx-xxxx (F.L.)

Abstract: This work focuses on the Lamb wave localization of damages within different anisotropic composite structures. The localization methods presented are based on the use of piezoelectric transducer networks, allowing the generation and reception of Lamb waves following their interaction with the damaged areas. In particular, the present contribution considers the case where the access to the reference state is not possible. In that case, baseline signals are constructed from a numerical simulation model using the previously determined elasticity tensor of the structure. However, since the latter tensor is not always easy to obtain in the case of anisotropic materials, the present work proposes the use of a second PZT network placed in a healthy zone of the studied structure. Signals related to the generated Lamb waves in different directions can therefore be considered for longer distances. This is performed by translating signals according to a simplified theoretical propagation model of Lamb waves in homogeneous structures. This work shows that based on the aforementioned baseline free methods, reliable images of damaged areas can be obtained in the case of transversely isotropic, unidirectional and quasi-transversely isotropic composites with the help of the delay-and-sum algorithm.

Keywords: Structural Health Monitoring, PZT network, Lamb waves, anisotropic composite structures, impact damage, delay-and-sum

Citation: Nzouatchoua, C.; Bentahar, M.; Montresor, S.; Colin, N.; Trottier, C.; Terrien, N. Damage localization on composite structures using new methods based on the delay-and-sum algorithm. *Sensors* **2022**, *1*, 0. https://doi.org/

Received:
Accepted:
Published:

1. Introduction

Maintenance operations are periodically carried out in industrial environments using non-destructive testing (NDT) techniques to ensure the reliability of structures. However, these techniques often have several disadvantages, such as the immobilization of the structure to be inspected throughout the inspection, the need for qualified operators, and long inspection times, depending on the dimensions to be inspected. A new multidisciplinary approach called Structural Heath Monitoring (SHM) is becoming increasingly popular in the aerospace, nuclear, shipbuilding, automotive, energy and civil engineering industries. The objective of SHM is to develop autonomous systems for continuous monitoring, inspection and damage detection of structures with minimal manpower involvement [1]. Two types of methods can be distinguished in the practice of SHM: passive methods in which sensors measure the response of the structure continuously and monitor their evolution with respect to the given thresholds, and active methods which, in addition to sensors, use actuators that generate stress waves to interrogate the structure. Among the active methods, the ones based on the use of guided ultrasonic waves have proven to be interesting and effective [2]. In the case of plate-like structures, Lamb waves can be generated, where the

free surfaces of the plate act as guides for the propagating Lamb waves in two types of modes: symmetric (S) and anti-symmetric (A) [3]. Lamb waves have the advantage of propagating over long distances with low attenuation. They can also interact with damages of wavelength size. However, one should be aware of their dispersive character which is in fact geometrical in nature. For practical reasons, often related to the interpretation of results, the fundamental Lamb modes A0 and S0 are used. The S0 mode has a higher sensitivity to structural thickness damage such as delamination, while the A0 mode has a higher sensitivity to surface damage such as cracking or corrosion [4]. In the case of a sensor network, the Lamb wave inspection is based on the use of several sensors, each of which plays the role of transmitter and receiver in an alternating way. Depending on the sensors' distribution, Lamb waves can interact in different ways (reflection, scattering) with existing damages within the structure. Signal processing is then performed to the collected signals in order to extract time and/or frequency domain signatures of the damages such as (time of arrival, amplitude, energy, etc.). Based on the different signatures, different imaging algorithms can be used to detect and locate the damage within the inspection area. In general, PZT sensors are very often used in Lamb wave inspections and can be tuned to generate only one Lamb mode of interest [5, 6].

There are several works in the literature dealing with Lamb wave damage localization using PZT arrays on aluminum and composite plates [7–11]. In general, these works are based on the extraction of a specific Damage Index (DI) from the detected signals. Several algorithms can therefore be implemented to perform the localization of the different damages by imaging the inspection area delimited by the PZT sensors. Some algorithms are based on the monitoring of the same inspection area for the same sensors' positions. This can be performed by first acquiring a baseline of reference signals related to the initial or reference state in which the structure is healthy. The, new measurements of the subsequent state of the structure (possibly a damaged state) are compared to the baseline signals and any significant change above the previously defined threshold is considered as a sign of an existing anomaly [12]. Residual signals, corresponding to the difference between the damaged and reference states' signals, are therefore in the imaging algorithms. Lamb wave tomography [13–16] is a good way to quantitatively evaluate damage imaging reconstruction but requires a high number of transducers. A simple example is the reconstruction algorithm based on the probabilistic damage inspection called RAPID. The latter uses the correlation between the signals taken at the reference and damaged states, which is quantified statistically by the Signal Difference Coefficient (SDC) [17]. Despite the need of a large number of transducers, the algorithm has the advantage of being free from the knowledge of the velocities corresponding to the involved Lamb modes. For this RAPID algorithm, the shape of the PZT array distribution also has a great influence on the imaging quality. Indeed, a good PZT distribution is the one that allows to have a homogeneous actuator-sensor path flow in the inspection area, thus avoiding focusing points that are sources of artefacts in the final image. A circular shape of the PZT array can provide optimal results [18]. A normalization factor is introduced to compensate the effect of the shape of the PZT network in [19]. In such a case, a constant form factor can also be changed to a variable parameter depending on the positions of the transmitter-receiver pairs as was done in [20]. Hua et al. [21] optimised the RAPID algorithm by transforming the SDC into LSDC (Local Signal Difference Coefficient), a new parameter that uses optimal signal lengths. On the other hand, algorithms based on the sparse reconstruction, i.e. exploiting the sparse nature of faults, are also used to detect defects with Lamb waves. These algorithms attempt to find a small set of locations that might contain damage consistent with the residual signals [22, 23]. However, they have the difficulty of having to analytically construct a wave dictionary. The delay-and-sum (DAS) algorithm, adopted from the radar community, is known to be very reliable. It is based on the exploitation of the residual signals and the group velocities of the propagating Lamb modes. The residual signals from all employed transmitter-receiver paths are shifted

according to an appropriate time-shift rule and then summed up to give an average signal [24, 25].

Baseline algorithms are often criticized for not taking into account environmental conditions such as temperature during the acquisition of Lamb signals at different states. Despite the existence of temperature compensation methods [26], one should note that it is not always possible to have a baseline state at which the structure is healthy, especially on operational structures. In such a case, the current trend is to develop methods without a reference state, where only measurements in the current state are taken into account and a prior knowledge of the structure is not necessary. Methods using time reversal [27, 28] are considered as baseline-free. They are based on the spatial reciprocity and time invariance of linear wave equations. The operation of time reversal of a signal in the time domain is equivalent to taking the complex conjugate of the Fourier transform of the signal in the frequency domain. Other baseline-free methods are based on baseline algorithm except that the reference state is constructed by exploiting measurements of the current or damaged state. Salmanpour et al. [29] present a method in which, by symmetrizing the distribution of the PZT array to divide the inspection region into symmetrical areas, the reference state is constructed simultaneously with the damaged state by considering only the healthy areas. DAS algorithm is then applied for localization. In [30, 31], baseline-free methods ERAPID and nonlinear RAPID inspired by the baseline algorithm RAPID are also presented. The present paper presents two methods in which the baseline signals are obtained in different ways. The first method is based on the 3D numerical simulation results performed using the SHM module of the CIVA software. The second method uses an analytical construction based on a simple theoretical propagation model of the elastic guided waves. In both methods, mixed residual signals are obtained and used to image damaged areas with the delay-and-sum algorithm. The first sample studied in this paper is a transverse isotropic composite plate. The latter which has been previously impacted was characterized to explore the possibility of modelling impact damage as conical shaped geometries with degraded mechanical properties (details of this work can be found in [32]). The second sample is a curved piece of a wind turbine blade. The latter is a composite-foam-composite sandwich, impacted away from the center. The third sample is a quasi-transversely isotropic composite plate impacted around its center. For the last two samples, the elastic properties, draping and material symmetry were not a priori known. The characterization of these materials and the damaged areas will be presented in this paper as follows: section 2 describes the different methods used, sections 3, 4 and 5 describe the work carried out and a discussion of the results related to aforementioned composite samples, and section 6 is the conclusion.

2. Damage localization methods based on delay-and-sum algorithm

This section presents the methods that are applied to structures that were previously damaged, for which no reference or healthy state data are available. The methods are based on the use of PZT network to delineate the inspection area containing damage. Structures are discretized into uniform grids of regularly spaced pixels. Images are obtained by calculating the contrast values at each pixel based on the probability of presence/ absence of damage at the different locations. The fundamental Lamb modes A0, S0 and SH0, are used for the reconstruction of the different images. The methods presented below use the delay-and-sum algorithm and are adjusted to take into account the anisotropy of the composite structures.

2.1. Simulation method

The method presented Figure 1, is based on the characterization of an already damaged composite plate. By identifying the elasticity tensor elements, reference state signals (i.e. for the healthy structure) related to the propagating Lamb waves were obtained with the help of numerical simulations performed using CIVA software [33, 34]. Simulations take into account the real experimental configuration (plate geometry, excitation signal

and frequency, number of PZTs, scan configuration, dimensions and positions of the PZT sensors, sampling frequency, acquisition or simulation time). Then, simulation results are subtracted from the experimentally obtained signals in the damaged state in order to obtain residual signals containing the damage signature. The last step of the proposed method is the application of the delay-and-sum algorithm to image the inspection area.

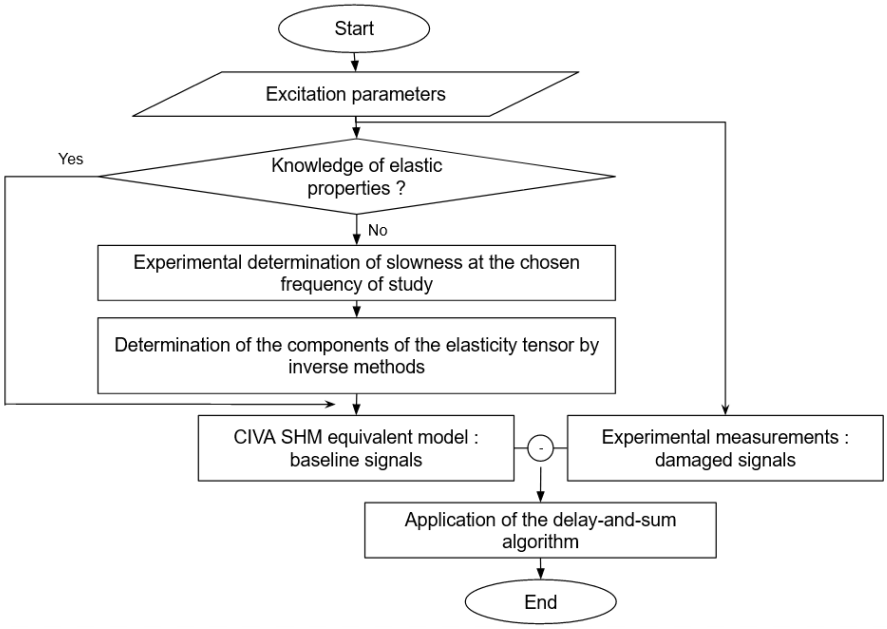

Figure 1. Method 1 based on the construction of the baseline signals by numerical simulations.

2.2. Experimental method

The first method uses a numerical simulation model to construct the reference or baseline state signals, in which the excitation parameters are exactly the same as in the experimental determination of the damaged state signals. However, one should be aware that the computation time can be very long, and the real propagation conditions in terms of "wave/structure" interaction are not always easy to implement. Furthermore, the determination of the elastic constants by inverse method remains a delicate task, despite the existence of various approaches just like the one based on the lamb waves [35, 36]. In general, as in composites, the sparse nature of the damage makes the density of the damaged areas low compared to the healthy areas [37]. This makes possible to find a healthy area and place a second PZT array in the same layout as the main PZT array, which covers the whole inspection zone. In the second method Figure 2, a second array is used to acquire intermediate signals. Xu et al. describe a theoretical approach of Lamb waves propagation model [38]. The latter is applied and adapted to our study in order to obtain the reference state signals from the intermediate signals, as described below.

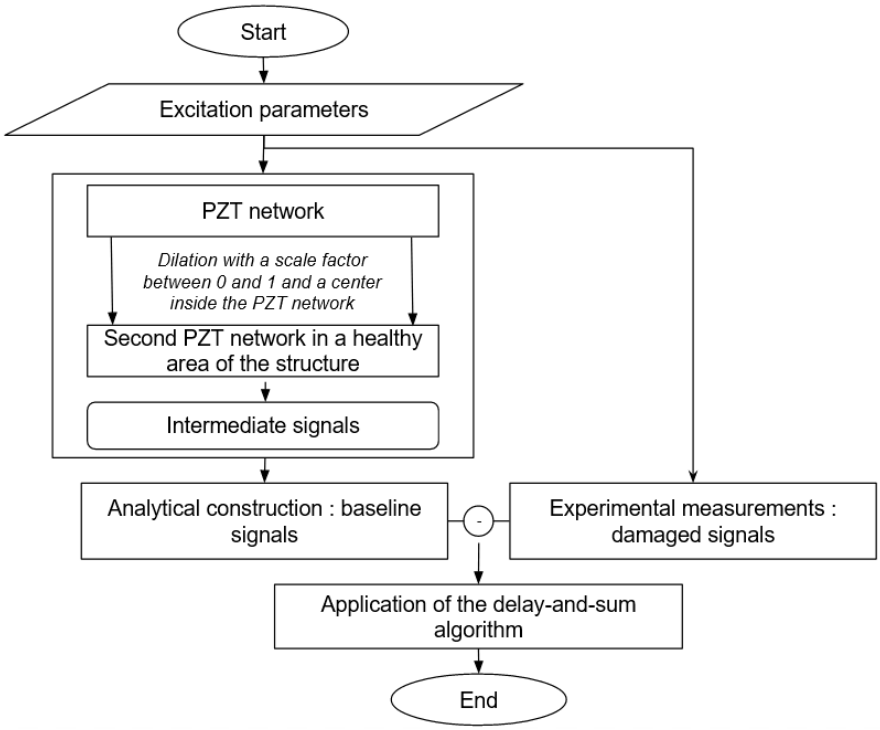

Figure 2. Method 2 based on an analytic construction of the baseline signals.

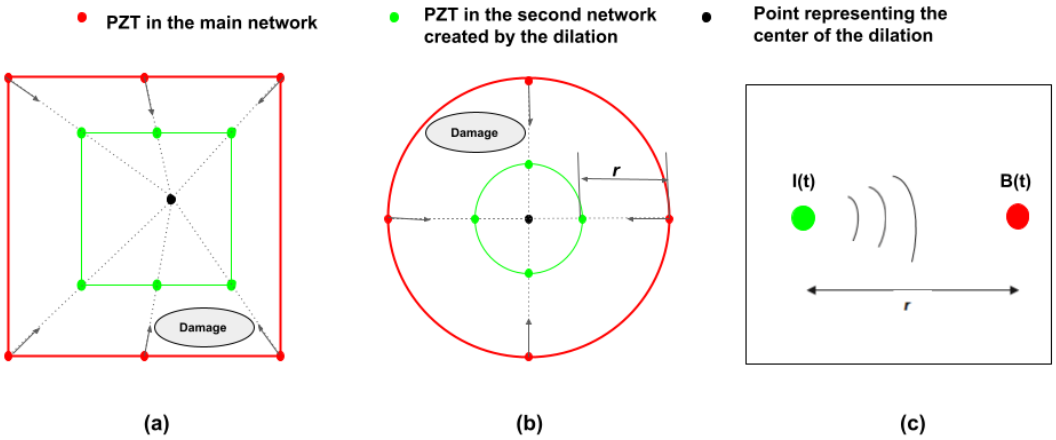

Figure 3. Method 2 baseline signals creation process : (**a**) dilation of a square distribution of six PZT . (**b**) dilation of a circular distribution of four PZT . (**c**) From intermediate signal to baseline signal.

It is assumed that a distance r in Figure 3(c) separates each PZT in the main network and its correspondent in the second network of PZTs. The complex signal of I(t) can be written as :

$$S(t) = I(t) * \exp(iw_c t) \tag{1}$$

With w_c the centre frequency of the excitation signal. In the frequency regime, we have:

$$S(w) = \int_{-\infty}^{+\infty} S(t) * \exp(-iwt)dt \tag{2}$$

or:

$$S(w) = \int_{-\infty}^{+\infty} I(t) * \exp[(-i(w - w_c)t]dt \quad (3)$$

We can therefore write :

$$S(w) = I(w - w_c) \quad (4)$$

The frequency signal corresponding to B(t) can be expressed as :

$$B(w) = \frac{1}{\sqrt{r}} * S(w) * \exp(-ik(w)r) \quad (5)$$

In the time domain, we have:

$$B(t) = \frac{1}{\sqrt{r}} * TF^{-1}\{I(w - w_c) * \exp(-ik(w)r\} \quad (6)$$

We assume linearity of the wavenumber as a function of frequency, i.e. we place ourselves in a region of low dispersion on the Lamb wave dispersion curve and we can write in the vicinity of w_c :

$$k(w) = \alpha + \beta(w - w_c) + 0(w - w_c) \quad (7)$$

With,

$$\alpha = k(w_c) = \frac{w_c}{V_p(w_c)} \text{ and } \beta = k'(w_c) = \frac{dk(w)}{dw} \mid (w = w_c) = \frac{1}{V_g(w_c)} \quad (8)$$

Where V_p and V_g represent the phase velocity and group velocity of the Lamb mode under consideration, respectively. The term 0(w-w_c) and higher order terms are considered as interference terms and are neglected. This gives :

$$B(t) = \frac{1}{\sqrt{r}} * TF^{-1}\{I(w - w_c) * \exp[-i(\alpha + \beta(w - w_c))r]\} \quad (9)$$

By calculating the inverse Fourier transform, we obtain :

$$B(t) = \frac{1}{\sqrt{r}} * exp(-i\alpha r) * \ exp(iw_c t) * \ I(t - \beta r) \quad (10)$$

By including the signal S(t) in this equation, it follows that:

$$B(t) = \frac{1}{\sqrt{r}} * exp(-i\alpha r) * \ exp(iw_c \beta r) * \ S(t - \beta r) \quad (11)$$

The signal B(t) can be finally expressed as:

$$B(t) = \frac{1}{\sqrt{r}} * \left[\exp\left(-i\frac{r * w_c}{V_p(w_c)}\right) * \exp\left(i\frac{r * w_c}{V_g(w_c)}\right)\right] * S\left(t - \frac{r}{V_g(w_c)}\right) \quad (12)$$

This signal is the product of three terms, the first of which represents the attenuation of Lamb waves proportional to the inverse of the square root of the distance travelled; the second term containing exponentials is independent of time and represents the phase variation; it cancels out when the phase velocity is equal to the group velocity; the third term corresponds to a time shift due to propagation.

2.3. Delay-and-sum algorithm applied to anisotropic materials

An illustration for a single pair of PZTs between transmitter i of coordinates (x_i,y_i) and receiver j of coordinates (x_j,y_j) is given Figure 4. It can be seen that the corresponding residual signal in time domain RES_{ij} (t) is delayed by passing it through the pixel P of coordinates (x_P,y_P). If the PZT array used contains a number N_T of PZTs, the same is true for all pairs used in the acquisitions, giving rise to a number N_S of signals. Each pixel in

the mesh undergoes this action and the contrast value at pixel P, for example, is obtained by the following formula:

$$I_P(x_P, y_P) = \frac{1}{N_s} \sum_{i=1}^{N_T-1} \sum_{j=i+1}^{N_T} ERES_{ij}\left(t_{ij}(x_P, y_p, \alpha)\right) \tag{13}$$

Where $ERES_{ij}$ is the envelope of the residual signal RES_{ij} between transmitter i and receiver j, and is obtained by a Hilbert transform. The time of flight t_{ij} (x_P,y_P,α) of the signal along the virtual path i-P-j is given by:

$$t_{ij}(x_P, y_p, \alpha) = \frac{d_{i-P}}{V_g(\alpha_{i-P})} + \frac{d_{P-j}}{V_g(\alpha_{P-j})} \tag{14}$$

The anisotropy in composite materials means that the group velocity of the different propagated Lamb modes is not the same in all directions and therefore the geometric angles involved in 14, defined by:

$$\alpha_{i-P} = \tan^{-1}\left|\frac{y_P - y_i}{x_P - x_i}\right| \text{ and } \alpha_{P-j} = \tan^{-1}\left|\frac{y_P - y_j}{x_P - x_j}\right| \tag{15}$$

Similarly, the distances d_{i-P} and $d_P - j$ represent respectively the distance between transmitter i and pixel P, and that between pixel P and receiver j; they are defined by:

$$d_{i-p} = \sqrt{(x_P - x_i)^2 + (y_P - y_i)^2} \text{ and } d_{p-j} = \sqrt{(x_P - x_j)^2 + (y_P - y_j)^2} \tag{16}$$

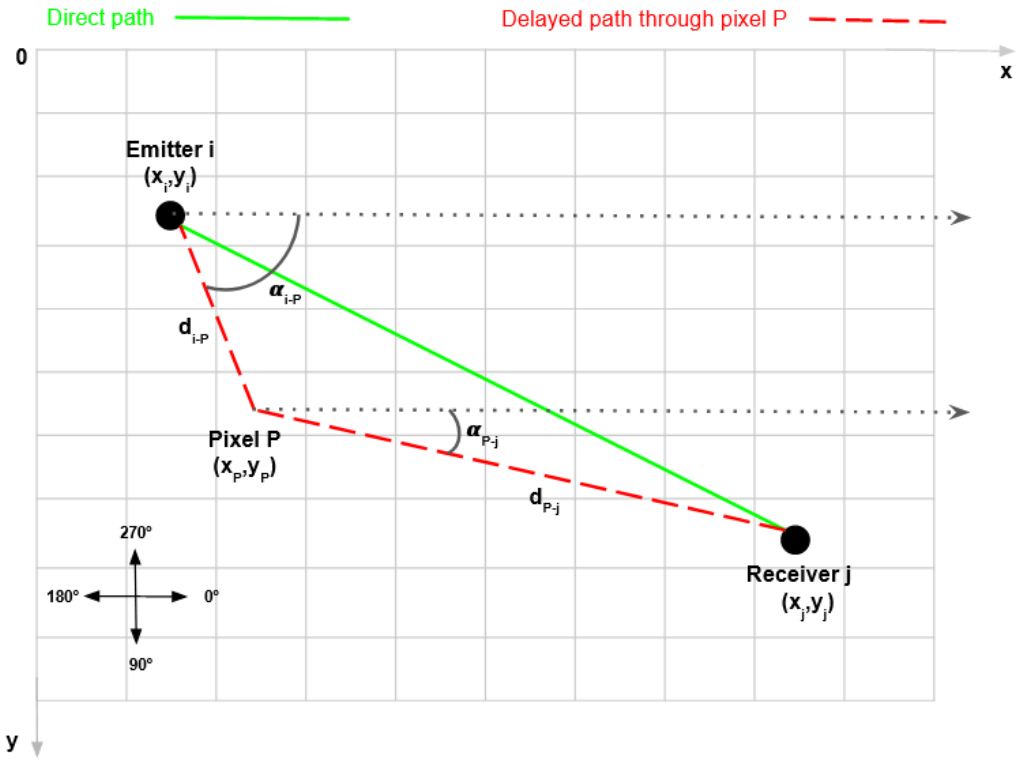

Figure 4. Delay-and-sum algorithm used in the two methods.

The pixels with the highest contrast values are the ones where the damage is located.

3. Transverse isotropic composite plate

The CFRC composite plate sample consists of 20 plies of 0.3 mm thickness sheets along the sequence $[45/0/0/45/0/45/0/45/0/45]_S$. The plate is transverse isotropic, where the axis of symmetry is along the thickness direction. Dimensions of the plate are of 500 × 500 x 6.2 mm3. As announced in the introduction, this plate was the subject of a previous study [32] during the optimised dispersion curves and elastic constants were determined experimentally Table 1. An impact was also made at the centre of this plate by means of a hemispherical impactor injecting thus an energy of 40 joules. In practice, impacts on composite structures occur when the structure collides or is struck by an external object. Very common examples of impacts are dropping of tools during the manufacturing, preparation or storage of the structure, or during use in service, e.g. for aeronautical components, bird strikes, hail etc. These impacts create damage that is hardly visible on the outer surfaces but which progresses through the thickness of the structure leading to local degradation of the mechanical properties around the impact location [39, 40]. The problem of locating damage in this case is to determine a damaged area surrounding the impact site. An ultrasonic C-scan was therefore performed around the impacted area to estimate the extent of the area to be located.

Table 1. Homogenised elastic properties of the composite plate

$\rho(g/\mathrm{cm}^3)$	$\mathbf{C_{11}(GPa)}$	$\mathbf{C_{22}(GPa)}$	$\mathbf{C_{33}(GPa)}$	$\mathbf{C_{12}(GPa)}$	$\mathbf{C_{13}(GPa)}$	$\mathbf{C_{23}(GPa)}$	$\mathbf{C_{44}(GPa)}$	$\mathbf{C_{55}(GPa)}$	$\mathbf{C_{66}(GPa)}$
1.55 ±0.05	52.4 ±2%	12.6 ±2%	52.4 ±2%	3.1 ±2%	17.8 ±2%	3.1 ±2%	3.7 ±2%	17.3 ±2%	3.7 ±2%

3.1. Acquisitions at the damaged state

Generation and reception of Lamb waves in different directions was performed with the help of an acquisition system, that can also be wireless Figure 5. This system was developed by the CEA in partnership with the Gustave Eiffel University; has 8 multiplexed channels for transmission and 8 parallel channels for reception. 8 PZT sensors (20 mm in diameter and 0.52 mm thick) are glued to the upper free surface (Z=0mm) of the plate. The coordinates of the sensors are given in Table 2. The excitation signal is a 3-cycle Toneburst (20Vpp) with an excitation center frequency of 150 KHz associated with a hanning window. Its narrow band frequency content concentrates the energy around the central excitation frequency of the sensors, thus reducing the natural effects of Lamb wave dispersion.

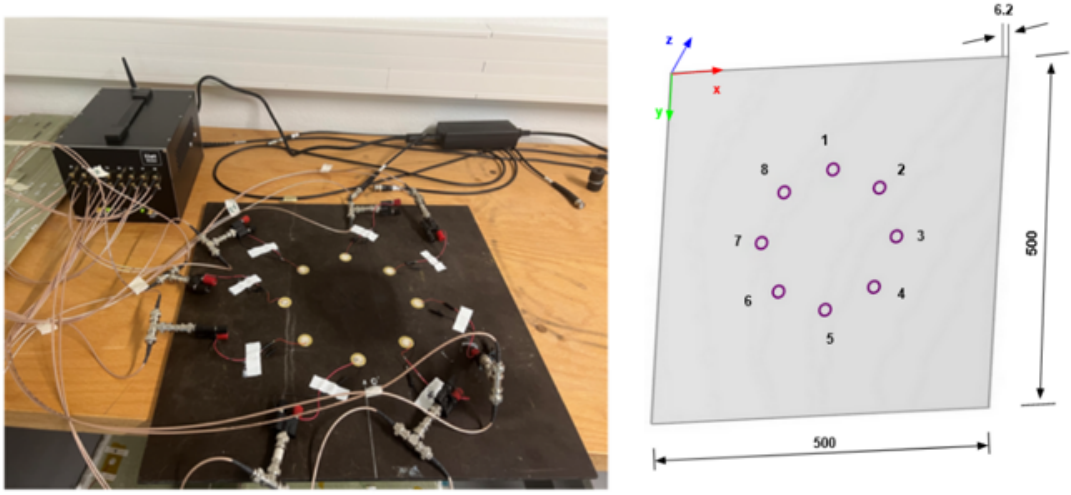

(a) (b)

Figure 5. experimental setup: (**a**) Wireless acquisition system . (**b**) orientation and plate dimension.

The scan is carried out in such a way that each sensor transmits in turn when the other sensors receive leading thus to 56 signals. The latter are acquired over a period of 500 µs, at a sampling rate of 2 MHz, which is 10 times greater than the excitation frequency.

Table 2. Coordinates of the PZT.

Positions	PZT1	PZT2	PZT3	PZT4	PZT5	PZT6	PZT7	PZT8
X (mm)	250	320	350	320	250	180	150	180
Y (mm)	150	180	250	320	350	320	250	180

3.2. CIVA modelling for the creation of the reference state

With the help of the elastic constants of the composite plate, dispersion curves corresponding to group velocities of fundamental Lamb modes were determined. Numerical simulations were performed in order to obtain signals corresponding to the transmitter-receiver pairs according to the scan configuration used. The reference state was thus numerically constructed using the following parameters:

1. The geometry and material properties of the plate (elasticity tensor, density). Although the arrangement of the plies is given, the plate is considered as homogeneous,
2. The positions and size of the PZTs, the excitation signal, are taken exactly the same as the experimental configuration.
3. The duration of the signals is the same as the acquisition time, i.e. 500 µs, and the sampling frequency is identical to the frequency used for the experiments.

3.3. Results and discussion

For the same transmitter-receiver pairs, 56 subtractions are performed between signals obtained experimentally at the damaged state and those obtained at the numerically simulated reference state. Envelopes of the obtained residual signals are then determined. An example of normalized signals taken at the reference (in blue) and damaged (in red) states are shown in Figure 6. The latter present the residual signals for an actuator-sensor pair whose path passes through the impacted zone (actuator 2 - sensor 6) and for a path not passing through it (actuator 3 - sensor 5).

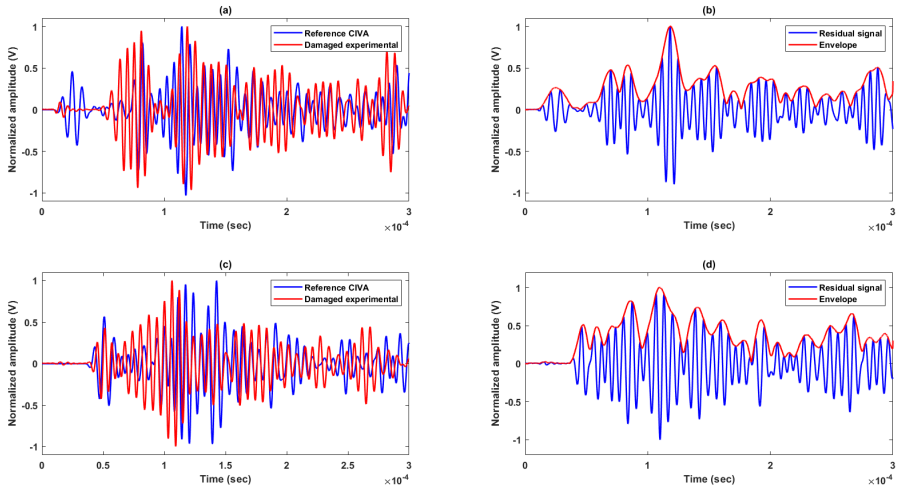

Figure 6. Baseline, damaged, residual and envelope of signals of two paths with one going through damage area and the other not: (**a**)Path (actuator 2 - sensor 6). (**b**)Path (actuator 2 - sensor 6). **c**)Path (actuator 3 - sensor 5). **d**)Path (actuator 3 - sensor 5).

The composite plate being anisotropic along the Z axis and isotropic in the (XY) plane, the speed of A0 and S0 modes can be considered as constant and have been respectively determined as 1650m/s and 5700m/s at the excitation frequency. The times of flight (TOF) in the different directions were consequently calculated based on these speeds. The result presented in Figure 7(a) is an image presenting the existing damage within the inspection area, obtained with a reconstruction based on the delay-and-sum algorithm assuming the A0 mode. Despite the complexity of the performed study, the localization of the defect zone is close to the one given by the ultrasonic C-scan as it can be seen in Figure 7(b). However, an improvement of the simulations can still be performed by taking into account, for example, the attenuation in order to limit the difference between the amplitudes of the simulated and experimental signals as well as their time shift [41].

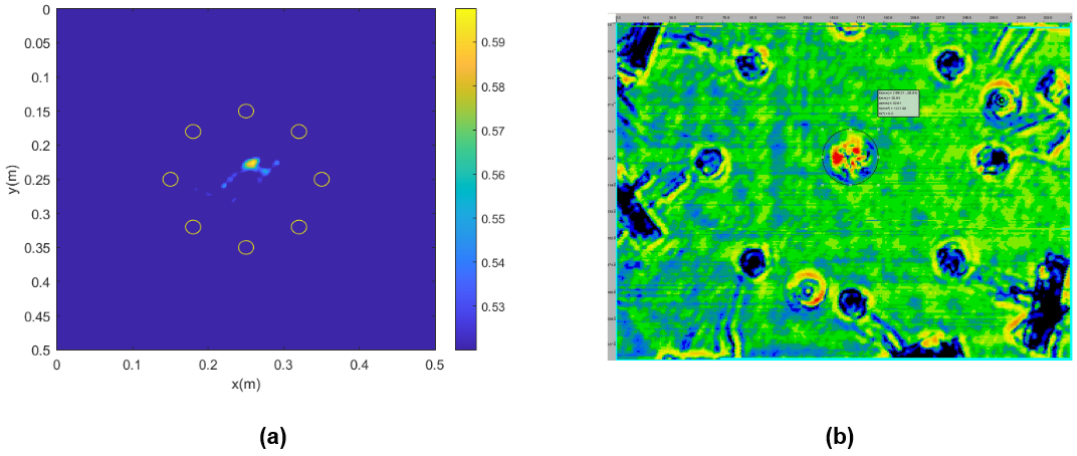

Figure 7. Damage localization results: (**a**) Method 1. (**b**) Ultrasonic C-scan.

4. Curved wind turbine blade sample

The structure studied here in Figure 8 is a piece of a wind turbine blade, of dimensions 600 x 500 x 45 mm3. It is a sandwich structure, consisting of the assembly two glass-fiber composite skins put on both sides of a foam core. Within such a structure, different types of damage can be present such as disbonds between the skin and the core or between the laminates of the skins, cracks in the skins and more general damage can be created by

impacts as it can be found in [42]. Due to the high thickness of the sandwich structure and the porous foam attenuation properties, lamb waves generated from the outer face have little chance to pass through the foam to be detected on the inner face of the wind turbine blade, even at high excitation amplitudes. For this reason, the present study is limited to the use of lamb waves to search for defects on the outer face of the wind turbine blade sample. The sandwich structure was impacted on the outer face. Contrary to many similar studies on composite structures found in the literature, in our case, we don't have any information on the draping and the material symmetry. Under these conditions, it is difficult to establish a 3D model representative of the experiment, as performed above. Furthermore, the structure has a curvature which should be taken into account. In order to better characterize the structure, a second array of sensors is placed away from the impacted area to acquire the intermediate signals. The latter are translated to obtain the reconstructed baseline signals.

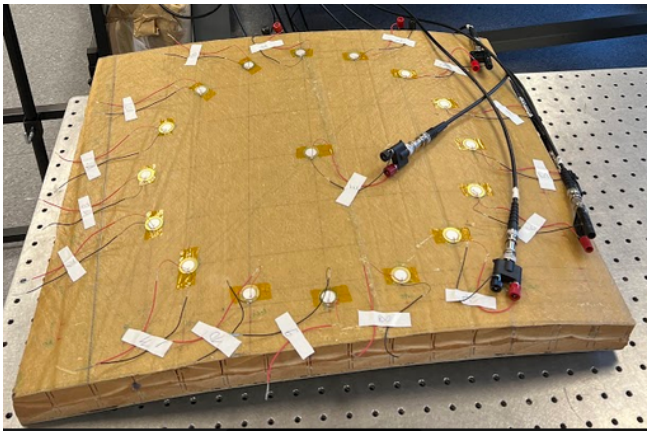

Figure 8. Curved wind turbine blade sample

4.1. Characterization of the wind turbine sample

In the absence of the necessary information regarding the propagation of Lamb waves within the sample, Lamb waves were generated in different directions with the help of a network of 16 sensors that forms a circle whose center is occupied by a transmitter transducer. Group velocities of the two fundamental modes A0 and S0 were therefore determined around the excitation frequency of 75kHz. For each direction, the direct modes (A0, S0) can be differentiated by their different slope characteristics with the help of the time-frequency representation [43]. A continuous wavelet transform is performed on the collected signals and the envelopes of the wavelet coefficients corresponding to the excitation frequency (75 KHz) are extracted to determine the different times of flight. Group velocities were calculated by taking into account the radius of curvature of the sample studied for the sensors' positions. An interpolation of the experimental data is then carried out to obtain the evolution of the group velocities with a step of 1°. The curves in Figure 9 represent the slowness of the S0 and A0 modes in the structure. It can be seen that the group velocity is maximum in the 0° direction and minimum along 90°. This allows to assume that the composite used is a unidirectional whose fibers would be oriented at 0°.

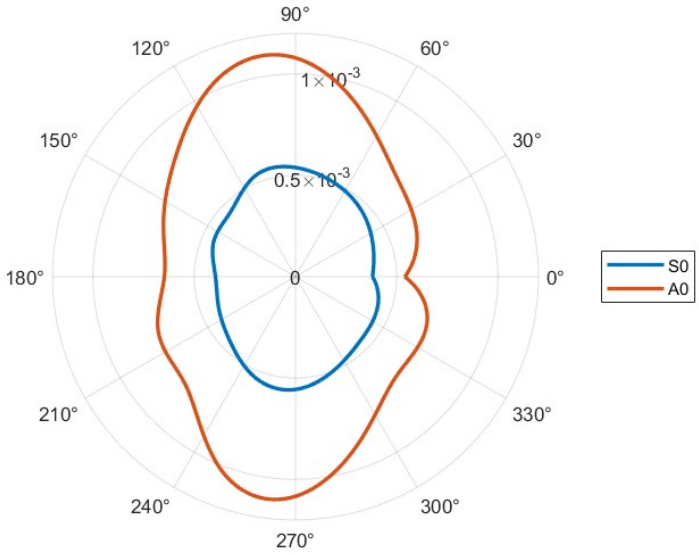

Figure 9. Slowness of S0 an A0 at the 75 KHz excitation frequency

4.2. Measurements and Reconstruction of the baseline signals

In view of the attenuation of Lamb waves when they propagate in the wind turbine blade, we had to amplify the excitation signals beforehand in order to ensure a good transmission of the signals especially when the waves cross the damaged zones. The excitation signal is a 3 cycle Tone burst delivered with a high amplitude of 400V to compensate for losses related to irregularities as well as roughness of the glass fiber composite. The excitation frequency was around 75 KHz, the sampling frequency used for the acquisitions was 20 MHz and the acquisition time was 2.5 ms. A circular sensors network of 400 mm diameter positioned in the center of the upper composite skin of the structure contains 16 PZT sensors of 20 mm diameter and 0.52 mm thickness. The coordinates of the sensors, which are uniformly arranged, are given in Table 3. The scan is carried out in such a way that each sensor transmits in turn when the other receive, thus giving rise to 240 signals.

Table 3. Coordinates of the PZT.

PZT	X(mm)	Y(mm)
1	450	300
2	434.8	376.5
3	391.4	441.4
4	326.5	484.8
5	250	500
6	173.5	484.8
7	108.6	441.4
8	65.2	376.5
9	500	300
10	65.2	223.5
11	108.6	158.6
12	173.5	115.2
13	250	100
14	326.5	115.2
15	391.4	158.6
16	434.8	223.5

Baseline signals were first obtained from the intact state in order to compare them with those obtained using the experimental method described in section 2.2. The new reference signals are obtained with the help of a second network of sensors deployed in the configuration shown in Figure 10. The latter is a reduced image of the main network

having the same center. Precautions are taken to ensure that this array is located in a zone of the inspection area that does not contain damages. The scan procedure is the same as the one performed with the main network, which includes the damaged area. This results in 240 intermediate signals; each signal obtained is then modified according to Equation 12. In practice, for each modified intermediate signal, the distance r in this equation is the difference between the path length in the main network and the path length in the secondary network; the term corresponding to the product of the exponentials is considered to be zero.

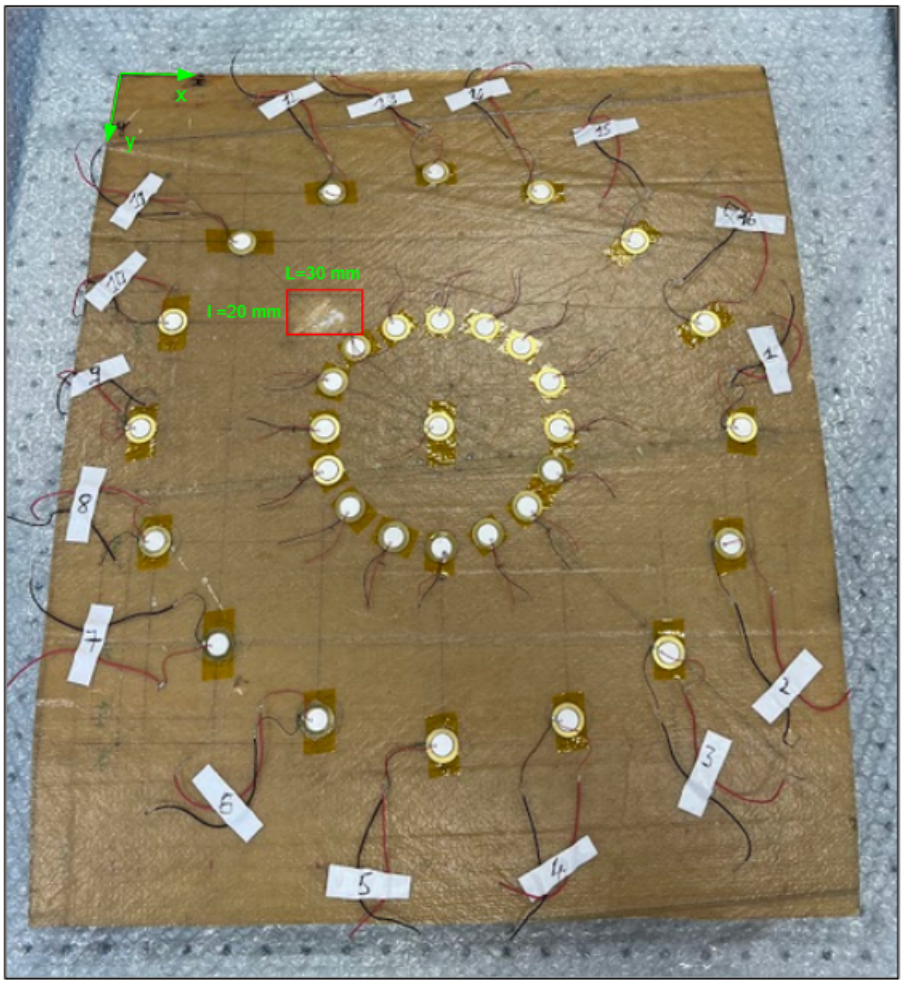

Figure 10. Dilation of the main PZT network for the acquisition of intermediate signal

4.3. Results and discussion

Figure 11 presents the results related to images obtained using the baseline signals taken at the initial intact state with the same sensors. The comparison between the two signals obtained in the intact and impacted states does not a priori allow to notice the difference which could exist between both states, even for signals which pass through the damaged zone as is the case in figure Figure 11(a). According to literature, for damage types corresponding to delamination and/or "fiber/matrix" breakage which are created during the impact of composites, there would be no particular reflection coming from the damaged area. Instead, one should expect a small change in amplitude of the detected signals, such as the one presented in the same figure. This makes the detection of small impacts more complicated than cracks or through thickness holes as explained in these references [24, 44]. In our case, the small impact has been successfully detected using the delay and sum method Figure 11(b). However, for the abovementioned reasons (see also the damage in Figure 10), the contrast in the image between the healthy and damaged areas

is not as large as that which could be had in the case of an important acoustic impedance mismatch (ex. through thickness holes).

Based on these results, which will serve as a reference, we applied the experimental method described in section 2.2 in order to image the damaged area via the same network of sensors where the reference state is constructed using a secondary network. Figure 12(a) shows signals obtained for the same ultrasonic path as in Figure 11, where the phase and wave shape of the first mode (identified as S0 mode) overlap well. However, this is not exactly the case for the other modes, where clear differences appear in both shape and phase. Nevertheless, the image of the damaged area presented in Figure 12(b) is similar to that obtained earlier on the same sample. The contrast obtained in the latter is comparable to that presented in Figure 11(b) in accordance with the type of damage created by the impact. The presence of artefacts can be explained by the fact that reconstruction of signals was performed on the basis of the speed of S0 mode, which overestimates the time of arrival corresponding to A0 mode. The amplitude discrepancy is due to attenuation used which may not take int account the existing inhomogeneities within the structure.

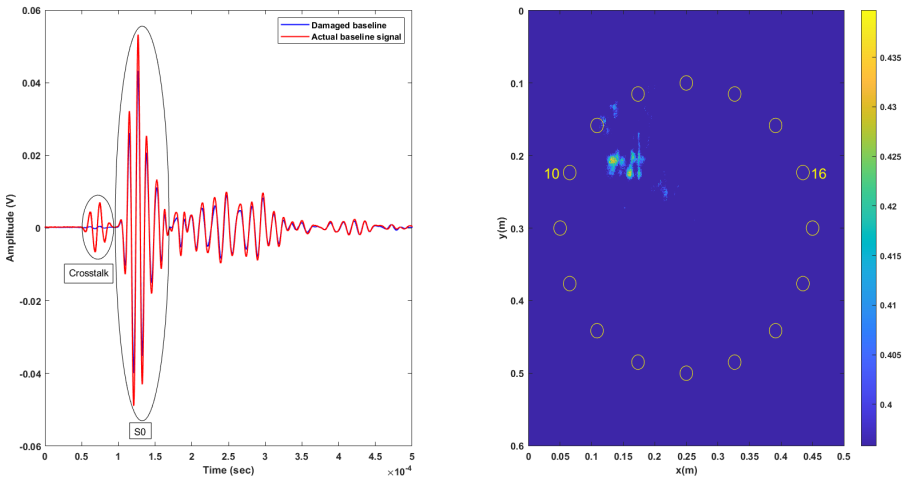

Figure 11. Damage localization results with delay and sum using actual baseline signals : (**a**) Actual baseline and damaged signals for (actuator 10 - sensor 16) going through damage area . (**b**)Reconstruction with S0 mode.

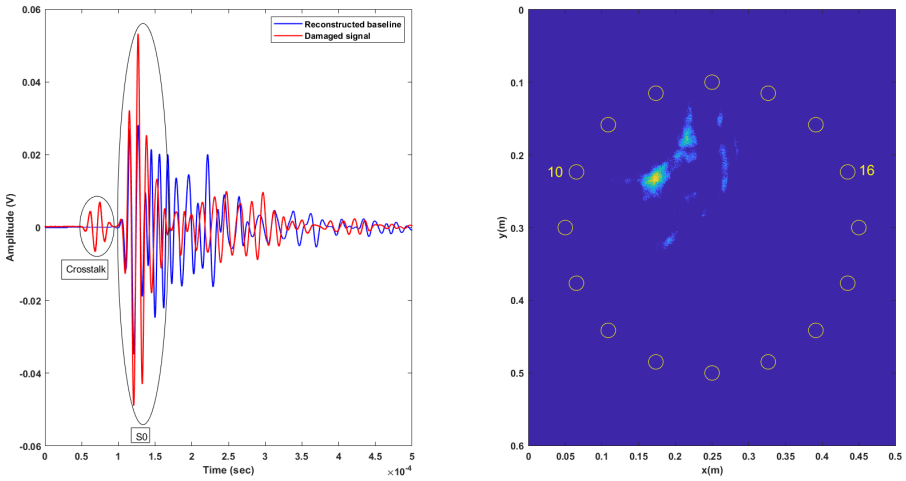

Figure 12. Damage localization results with method 2 using reconstructed baseline signals: (**a**) Reconstructed baseline and damaged signals for (actuator 10 - sensor 16) going through damage area. (**b**) Reconstruction with S0 mode. .

5. Anisotropic Carbon fiber composite plate

The third sample that has been characterized is a composite plate (600x600x3.5 mm3) for which information related to draping, symmetry and consequently elastic properties are not available. The present study aims to detect and locate the damage created by a prior impact on the aforementioned plate for which we do not have a healthy or pristine state. Furthermore, there is no quantitative information on the performed impact except its positioned at the center of the plate. In the following, group velocities of the generated Lamb waves are first determined based on scanning laser measurements. Then, intermediate signals are generated and detected based on a secondary network of PZT sensors before processing these signals using the experimental method described in section 2.2

5.1. Characterisation of the composite symmetry

Lamb waves are generated in different directions using an excitation frequency of 150 KHz. Scanning laser measurements were performed to pick-up the out-of-plane component of displacements according to the different directions that surround a transmitting transducer (area= 15x15 cm2) as shown in Figure 13(a). In view of the excitation frequency, wave packets were identified as S0, SH0, and A0 respectively. Indeed, after a propagation time corresponding to 65µs, the propagation of the wave packets was observed before the fastest wave is reflected on the edge of the plate or by the damaged area as shown in Figure 13(b). The latter also shows the diamond-shaped distribution of the Lamb wave velocities symmetrically between 0° and 360°. Two main directions of propagation were therefore identified, namely 0° and 90°, along which the velocity of the different modes is maximum, where VS0= 5712 m/s, VA0 = 1904 m/s and VSH0= 3808 m/s.

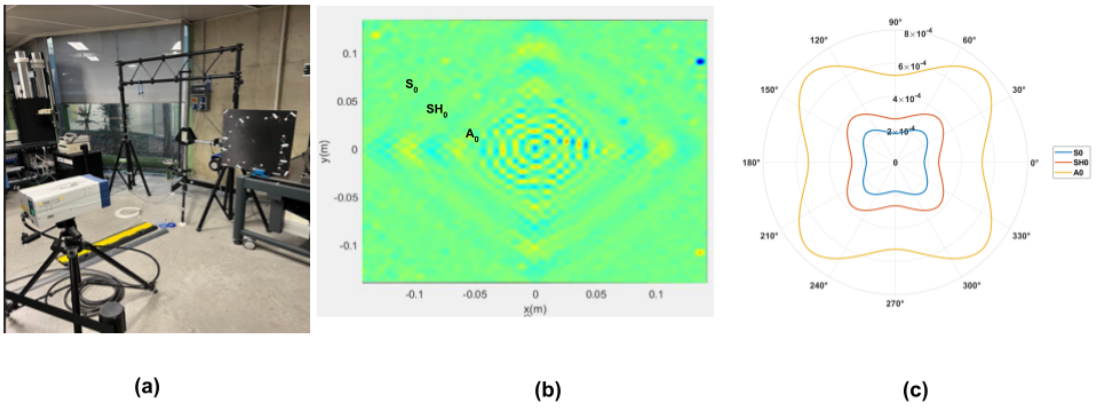

Figure 13. Characterization of anisotropy : (**a**) Schematic for measuring group velocities of A0, S0 and SH0 Lamb wave modes using laser. (**b**) Lamb Waves propagation after 65 µs. (**c**) Slowness of S0, SH0, A0 at the excitation frequency.

By collecting the velocities in different directions and then interpolating, a complete representation of the slowness curves for the three fundamental Lamb waves are obtained as presented in Figure 13(c). According to literature [45], and based on the experimental results, the symmetry of the composite plate was identified as quasi-isotropic-transverse. Indeed, this symmetry corresponds to an orthotropic symmetry invariant by a rotation of 90° around a single axis of the orthotropic reference frame and is characterized by six independent elasticity moduli [3, 4, 46].

5.2. Damaged state and baseline signals

In order to locate the damage within the anisotrpic composite plate, 12 evenly distributed PZT sensors are used to cover a square inspection area with an edge equal to 450 mm as shown in Figure 14. Lamb waves are generated around 150kHz with an amplitude corresponding to 30Vpp. The impact damage is situated in the center of the plate. The scan is carried out in the same way as described earlier to give 132 signals, which are acquired over a period of 500 µs at a sampling rate of 2 MHz.

In order to obtain the baseline signals, a second network is used to covers a square inspection area with an edge equal to 100 mm away from the impact. 132 intermediate signals are then obtained and modified according to Equation 12 with the same assumptions used before to construct the baseline signals.

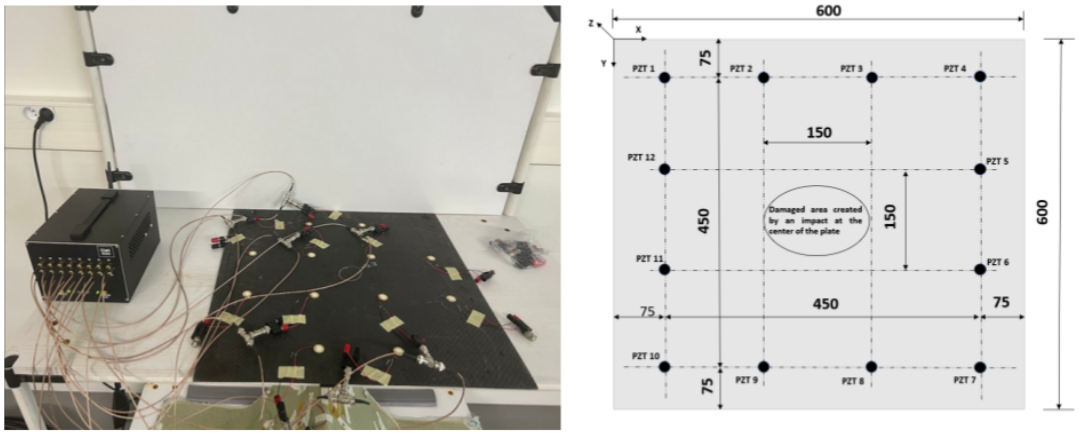

Figure 14. Schematic of the composite plate : (**a**) Experimental setup. (**b**) PZT locations and the damaged area.

5.3. Results and discussion

The visualisation of the signals in the reference and damaged states is presented in Figure 15. The latter shows a comparison of the reconstructed baseline signals (in red) and the damaged signals (in blue) when the ultrasonic path does not pass through the damaged area (Figure 15 (a)) and when it goes through it (Figure 15 (b)). Away from the defect area, a strong resemblance can be observed for the signals originating from the path between sensors 1 and 3. For the path between the sensors 6 and 12, it can be seen that the presence of damage has a visible effect that can be observed on almost all the signal in terms of amplitude and time shift.

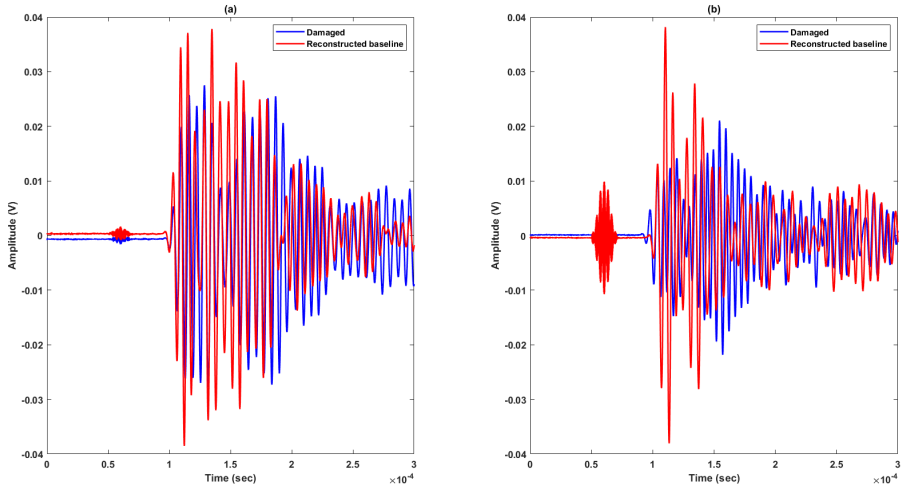

Figure 15. Method 2 signals of two paths with one not going through damage area and the other passing by : (**a**) Path 1-3. (**b**) Path 6-12.

Figure 16 presents the localization results obtained based on the delay-and-sum algorithm by considering the incident wave corresponding to A0, SH0 and S0 modes, respectively. The obtained images show a good agreement with the real impact location when the incident Lamb wave is taken as A0 and S0 with a remarkable accuracy. However,

results related to the case when the incident Lamb wave is taken as SH0 did not allow to obtain a successful localization. The significant change in the waveform shows that the wave packet related to the SH0 mode has been seriously affected by the interaction with the damaged area. The generated Lamb modes (A0, S0 or SH0) are expected to be either directly transmitted, reflected from an edge of the structure or damage or converted [46]. The time shift between wave packets in path 6-12 also suggests the possibility of mode conversion by damage in the plate [47]. Some conversions are well known such as the case of symmetric discontinuities with respect to the plate's mid-plane during which mode conversion only generates modes that share the same symmetry as the incident mode[48]. The reflection of the S0 mode from a delamination in crossply laminates with symmetric and asymmetric delamination showed that when A0 mode interacts with the delamination that is located asymmetrically across the thickness, the mode-converted S0 is observed. The mode-converted S0 mode revealed to be confined within the delamination region and converts back to A0 mode when delamination is symmetrically located across the thickness[49, 50]. According to their displacement profile across the plate's thickness, SH guided wave modes are classified between symmetric and antisymmetric. The interaction of SH waves with a discontinuity can be complex depending on the discontinuity shape as well as the operating frequency-thickness product[51, 52]. From the incidence of a single SH mode upon a thickness discontinuity (such as the one created by an impact) any mode can arise due to mode conversion. This makes the estimation of the conversion that took place very difficult in particular in an anisotropic material such as the composite plate studied. When using the delay-and-sum algorithm, mode conversion can be taken into account by differentiating the speed of the incident mode between the transmitter and the pixel and that of the converted mode between the pixel and the receiver in Equation 14. In the absence of any valuable information about the existing conversion, different combinations can be applied leading to a multi-modal reconstruction according to the involved propagating modes.

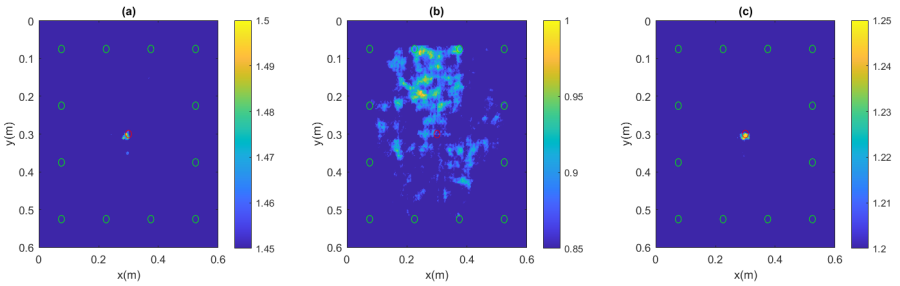

Figure 16. Damage localization with method 2: (**a**) Reconstruction with S0. (**b**) Reconstruction with SH0. (**c**) Reconstruction with A0.

6. Conclusions

In this paper, two contributions are made for the localisation of damages in composite structures for which no healthy state is available. The first method consists of obtaining baseline signals by a numerical simulation in which the same parameters are applied as in the acquisition of the damaged signals; the delay and sum algorithm then acts on the mixed residual signals to obtain the imaging. This method was applied to a transverse isotropic composite plate and the result is close to the ultrasound C-scan performed but can be perfect if the dispersion and attenuation in the plate are finely characterized. Furthermore, it is not always easy to access or even determine the elasticity tensor of the structure, which increases the complexity of this method. Thus, a first alternative to method 1 that could improve the result was to adapt the method used in [53] to our case; in fact, in this method, there is no residual signal because no baseline state is constructed, but only the measurements of the damaged state in pulse-echo mode are used. However, Lamb wave signals acquired in pulse-echo with the same PZT transmitting and receiving are very often corrupted because the PZT starts to receive the signal while the transmission

continues. Therefore, unlike the case here, where the PZTs are almost colocated to perform a pulse-echo scan, the exact same arrangement of the PZT array was placed on both free surfaces of the plate. If a PZT on the top surface transmits, its counterpart on the opposite surface receives; this action allowed us to make almost pulse-echo acquisitions. Such a method gives as many signals as there are PZTs on each side of the plate and is justifiable because the plane of polarisation of Lamb waves during their propagation always contains the direction along the thickness regardless of the direction of propagation and therefore any PZT on one of the free surfaces of the plate is able to transmit and receive the signal. The result obtained was indeed more accurate than Method 1 but was not subsequently confirmed for the other samples in this paper. Therefore, a second method is presented in this paper, which relies on a second PZT array placed in a healthy area of the structure, image from the first one by a dilation of positive ratio and less than 1 and with a center located in the main array. The second PZT array yields intermediate signals which by modification according to a simple theoretical Lamb wave propagation model lead to reconstructed baseline signals. As in method 1, the delay and sum algorithm then acts on the mixed residual signals to obtain the imagery. This method was first applied to a curved piece of wind turbine blade and then to a quasi-isotropic-transverse composite plate. In both cases it was shown that damages were well localized despite the attenuation and dispersion not being perfectly taken into account. Another strong point of the work presented in this paper is that we can use samples for which we don't have the mechanical characterisation, which is rarely the case in the literature. The key was to determine for the different modes used, the velocities or slowness between 0° and 360°, from PZT or laser, then to introduce in each case, the angle dependence in the delay and sum algorithm. The next steps in the work are to test the methods on more complex structures with stiffeners; then, in addition to localisation, it would be interesting to reconstruct the shape of the damage. For this, we are investigating how to couple the presented methods with Lamb wave factorisation methods.

Author Contributions: For research articles with several authors, a short paragraph specifying their individual contributions must be provided. The following statements should be used "Conceptualization, X.X. and Y.Y.; methodology, X.X.; software, X.X.; validation, X.X., Y.Y. and Z.Z.; formal analysis, X.X.; investigation, X.X.; resources, X.X.; data curation, X.X.; writing—original draft preparation, X.X.; writing—review and editing, X.X.; visualization, X.X.; supervision, X.X.; project administration, X.X.; funding acquisition, Y.Y. All authors have read and agreed to the published version of the manuscript.", please turn to the CRediT taxonomy for the term explanation. Authorship must be limited to those who have contributed substantially to the work reported.

Funding: Please add: "This research received no external funding" or "This research was funded by NAME OF FUNDER grant number XXX." and and "The APC was funded by XXX". Check carefully that the details given are accurate and use the standard spelling of funding agency names at https://search.crossref.org/funding, any errors may affect your future funding.

Institutional Review Board Statement: Not applicable

Informed Consent Statement: Not applicable

Data Availability Statement: In this section, please provide details regarding where data supporting reported results can be found, including links to publicly archived datasets analyzed or generated during the study. Please refer to suggested Data Availability Statements in section "MDPI Research Data Policies" at https://www.mdpi.com/ethics. If the study did not report any data, you might add "Not applicable" here.

Acknowledgments: In this section you can acknowledge any support given which is not covered by the author contribution or funding sections. This may include administrative and technical support, or donations in kind (e.g., materials used for experiments).

Conflicts of Interest: Declare conflicts of interest or state "The authors declare no conflict of interest." Authors must identify and declare any personal circumstances or interest that may be perceived as inappropriately influencing the representation or interpretation of reported research results. Any role

of the funders in the design of the study; in the collection, analyses or interpretation of data; in the writing of the manuscript; or in the decision to publish the results must be declared in this section. If there is no role, please state "The funders had no role in the design of the study; in the collection, analyses, or interpretation of data; in the writing of the manuscript; or in the decision to publish the results".

Sample Availability: Samples of the compounds ... are available from the authors.

Abbreviations

The following abbreviations are used in this manuscript:

MDPI	Multidisciplinary Digital Publishing Institute
DOAJ	Directory of open access journals
TLA	Three letter acronym
LD	Linear dichroism

Appendix A

Appendix A.1

The appendix is an optional section that can contain details and data supplemental to the main text—for example, explanations of experimental details that would disrupt the flow of the main text but nonetheless remain crucial to understanding and reproducing the research shown; figures of replicates for experiments of which representative data are shown in the main text can be added here if brief, or as Supplementary Data. Mathematical proofs of results not central to the paper can be added as an appendix.

Table A1. This is a table caption.

Title 1	Title 2	Title 3
Entry 1	Data	Data
Entry 2	Data	Data

Appendix B

All appendix sections must be cited in the main text. In the appendices, Figures, Tables, etc. should be labeled, starting with "A"—e.g., Figure A1, Figure A2, etc.

References

1. Chang, F.-K. Structural Health Monitoring: A Summary Report on the First Stanford Workshop on Structural Health Monitoring. English. *Report on the first stanford Workshop on structural,* 12 (Sept. 1997).
2. Raghavan, A. & Cesnik, C. E. Review of Guided-wave Structural Health Monitoring. English. *SAGE Publications* **39,** 91–114 (Mar. 2007).
3. ROYER, D. & DIEULESAINT, E. *Ondes élastiques dans les solides* MASSON. Français (1996).
4. Su, Z. & Ye, L. *Identification of Damages using Lamb waves* English (Lecture Notes in Applied and Computational Mechanics, 2009).
5. Giurgiutiu, V. & Soutis, C. Enhanced Composites Integrity Through Structural Health Monitoring. English. *Appl Compos Mater* **19,** 813–829 (Feb. 2012).
6. Lize, E. *Détection d'endommagement sans état de référence et estimation de la température pour le contrôle santé intégré de structures composites par ondes guidées* French. PhD thesis (Ecole nationale supérieure d'arts et métiers - ENSAM, Dec. 2018).
7. Diamanti, K., Soutis, C. & Hodgkinson, J. Piezoelectric transducer arrangement for the inspection of large composite structures. English. *Composites : Part A - Applied science and manufacturing* **38** (Jan. 2007).
8. Kessler, S. S. *Piezoelectric-based in-situ damage detection of composite materials for structural health monitoring systems* English. DOCTORATE OF PHILOSOPHY IN AERONAUTICS AND ASTRONAUTICS (MASSACHUSETTS INSTITUTE OF TECHNOLOGY, Jan. 2002).

9. Masurkar, F. & Yelve, N. Optimizing location of damage within an enclosed area defined by an algorithm based on the Lamb wave response data. *Applied Acoustics,* 13 (Jan. 2017).
10. SARAVANOS, D. A., HOPKINS, D. A. & BIRMAN, V. Detection of delaminations in composite beams using piezoelectric sensors. English. *35th Structures, Structural Dymimics, and Materials Conference* (Apr. 1994).
11. Kessler, S. S. & Spearing, S. M. DAMAGE DETECTION IN COMPOSITE MATERIALS USING LAMB WAVE METHODS. *Smart Materials and Structures* (Jan. 2002).
12. Sharif Khodaei, Z. & Aliabadi, M. H. F. English. in *Structural Health Monitoring for Advanced Composite Structures* Computational and Experimental Methods in Structures, 288 (Feb. 2018).
13. Wang, D., Zhang, W., Wang, X. & Sun, B. Lamb-Wave-Based Tomographic Imaging Techniques for Hole-Edge Corrosion Monitoring in Plate Structures. English. *materials,* 14 (Dec. 2016).
14. Leonard, K. R., Malyarenko, E. R. & Hinders, M. K. Ultrasonic Lamb wave tomography. English. *Inverse Problems* **18,** 15 (Aug. 2002).
15. Liu, Y., Zhou, S., Ning, H., Yan, C. & Hu, N. An Inverse Approach of Damage Identification Using Lamb Wave Tomography. English. *sensors* **19** (Oct. 2019).
16. ZHAO, X., ROYER, R. L., OWENS, S. E. & Joseph L, R. Ultrasonic Lamb wave tomography in structural health monitoring. English. *SMART MATERIALS AND STRUCTURES* **20** (Aug. 2011).
17. Zhao, X. & Rose, J. L. Ultrasonic guided wave tomography for ice detection. English. *Ultrasonics* **67,** 212–219 (Nov. 2015).
18. Wang, S., Wu, W., Shen, Y., Liu, Y. & Jiang, S. Influence of the PZT Sensor Array Configuration on Lamb Wave Tomography Imaging with the RAPID Algorithm for Hole and Crack Detection. English. *sensors* (June 2020).
19. Dziendzikowski, M., Dragan, K. & Katunin, A. Localizing impact damage of composite structures with modified RAPID algorithm and non-circular PZT arrays. English. *archives of civil and mechanical engineering* (Oct. 2016).
20. Sheen, B. & Cho, Y. A study on quantitative Lamb Waves Tomogram via modified RAPID Algorithm with shape factor optimisation. English. *INTERNATIONAL JOURNAL OF PRECISION ENGINEERING AND MANUFACTURING* **13,** 671–677 (Jan. 2012).
21. Hua, J., Lin, J. & Zeng, L. High-resolution damage detection based on local signal difference coefficient model. English. *Structural Health Monitoring* **14,** 20–34 (Dec. 2014).
22. Levine, R. M. *ULTRASONIC GUIDED WAVE IMAGING VIA SPARSE RECONSTRUCTION* English. PhD thesis (Georgia Institute of Technology, Jan. 2014).
23. Levine, R. M. & Michaels, J. E. Model-based imaging of damage with Lamb waves via sparse reconstruction. English. *Acoustical Society of America* **133,** 1525–1534 (Mar. 2013).
24. Sharif-Khodaei, Z. & Aliabadi, M. H. Assessment of delay-and-sum algorithms for damage detection in aluminium and composite plates. English. *Smart Mater. Struct.* **23** (May 2014).
25. E Michaels, J. Detection, localization and characterization of damage in plates with an in situ array of spatially distributed ultrasonic sensors. English. *SMART MATERIALS AND STRUCTURES* **17** (May 2008).
26. Salmanpour, M., Khodaei, Z. S. & Aliabadi, M. Guided wave temperature correction methods in structural health monitoring. English. *Journal of Intelligent Material Systems and Structures* **28(5),** 604–618 (2017).
27. Park, H. W., Sohn, H., Law, K. H. & Farrar, C. R. Time reversal active sensing for health monitoring of a composite plate. English. *Journal of Sound and Vibration* **302** (Jan. 2007).
28. Park, H. W., Kim, S. B. & Sohn, H. Understanding a time reversal process in Lamb wave propagation. English. *Wave Motion* **46,** 451–467 (Sept. 2009).
29. Salmanpour, M. S., Khodaei, Z. S. & Aliabadi, M. H. Instantaneous Baseline Damage Localization Using Sensor Mapping. English. *IEEE SENSORS JOURNAL* **17** (Jan. 2017).
30. Sun, H., Zhang, A., Wang, Y. & Qing, X. Baseline-free damage imaging for metal and composite plate-type structures based on similar paths. English. *International Journal of Distributed Sensor Networks* **15** (Mar. 2019).
31. Hettler, J., Tabatabateipour, M., Delrue, S. & Van Den Abeele, K. Application of Probabilistic Algorithm for Ultrasonic Guided Wave Imaging of Carbon Composites. English. *Physics Procedia* **70,** 664–667.

32. Singh, D., Mechri, C., El Guerjouma, R. & Bentahar, M. 3D Modelling of the Scattering of the Fundamental Anti-Symmetric Lamb Mode (A0) Propagating within a Point-Impacted Transverse-Isotropic Composite Plate. English. *applied sciences* **11** (July 2021).
33. Mesnil, O., Imperiale, A., Demaldent, E. & Chapuis, B. Validation of spectral finite element simulation tools dedicated to guided wave based structure health monitoring. English. *AIP Conference Proceedings* **38** (Aug. 2019).
34. *CIVA SHM* https://www.extende.com/files/extende/download_files/Discover_CIVA_SHM.pdf.
35. Han Orta, A. *et al.* Characterization of orthotropic elastic tensor using lamb waves. English. *Forum Acusticum,* 3319–3326 (2020).
36. Kudela, P., Radzienski, M., Fiborek, P. & Wandowski, T. Elastic constants identification of fibre-reinforced composites by using guided wave dispersion curves and genetic algorithm for improved simulations. English. *Composite Structures* **272** (May 2021).
37. Wang, W., Bao, Y., Zhou, W. & Li, H. Sparse representation for Lamb-wave-based damage detection using a dictionary algorithm. English. *Ultrasonics 87 (2018),* 48–58 (Oct. 2018).
38. Xu, C., Yang, Z., Tian, S. & Chen, X. Lamb wave inspection for composite laminates using a combined method of sparse reconstruction and delay-and-sum. English. *Composite Structures* **223** (Nov. 2019).
39. Abbas, S., Jianxi, Q. & Li, F. A Review on SHM Techniques and Current Challenges for Characteristic Investigation of Damage in Composite Material Components of Aviation Industry. English. *ASTM* **7,** 224–258 (June 2018).
40. Castaings, M., Singh, D. & Philippe, V. Sizing of impact damages in composite materials using ultrasonic guided waves. English. *NDT&E International* **46,** 22–31 (Oct. 2011).
41. De Luca, A., Caputo, F., Sharif Khodaei, Z. & Aliabadi, M. Damage characterization of composite plates under low velocity impact using ultrasonic guided waves. English. *Composites Part B* **138,** 168–180 (2018).
42. Li, X., Yang, Z. & Chen, X. Quantitative Damage Detection and Sparse Sensor Array Optimization of Carbon Fiber Reinforced Resin Composite Laminates for Wind Turbine Blade Structural Health Monitoring. English. *Sensors* **14,** 7312–7331 (Apr. 2014).
43. Li, F., Meng, G., Ye, L., Lu, Y. & Kageyama, K. Dispersion analysis of Lamb waves and damage detection for aluminum structures using ridge in the time-scale domain. English. *Sci. Technol,* 11 (July 2009).
44. Zhao, X. *et al.* Active health monitoring of an aircraft wing with embedded piezoelectric sensor/actuator network: I. Defect detection, localization and growth monitoring. English. *SMART MATERIALS AND STRUCTURES* **16,** 1208–1217 (2007).
45. CHEVALIER, Y. Comportements élastique et viscoélastique des composites. French. *Techniques de l'Ingénieur, traité Plastiques et Composites.*
46. Lammering, R., Gabbert, U., Sinapius, M., Schuster, T. & Wierach, P. *Lamb-Wave Based Structural Health Monitoring in Polymer Composites* English (Springer International Publishing AG 2018, 2018).
47. Jia, H. *et al.* A baseline-free approach of locating defect based on mode conversion and the reciprocity principle of Lamb waves. English. *Ultrasonics* **102** (Jan. 2020).
48. Kubrusly, A. C., Tovar, P., von der Weid, J. P. & Dixon, S. Mode conversion of SH guided waves with symmetry inversion in plates. *Ultrasonics* **112** (2021).
49. Ramadas, C., Balasubramaniam, K., Joshi, M. & Krishnamurthy, C. V. Numerical and experimental studies on propagation of A0 mode in a composite plate containing semi-infinite delamination: Observation of turning modes. English. *Composite Structures* **93,** 1929–1938 (2011).
50. Ramadas, C., Balasubramaniam, K., Hood, A., Joshi, M. & Krishnamurthy, C. V. Modelling of attenuation of Lamb waves using Rayleigh damping: Numerical and experimental studies. English. *Composite Structures* **93,** 2020–2025 (2011).
51. Kubrusly, A. C., Freitas, M. A., von der Weid, J. P. & Dixon, S. Interaction of SH guided waves with wall thinning. English. *NDT and E International* (2018).
52. Nurmalia, Nakamura, N., Ogi, H., Hirao, M. & Nakahata, K. Mode conversion behavior of SH guided wave in a tapered plate. English. *NDT&E International* **45,** 156–161 (2012).
53. Hameed, M. S., Li, Z. & Zheng, K. Damage Detection Method Based on Continuous Wavelet Transformation of Lamb Wave Signals. English. *applied sciences* (Jan. 2020).